On the sensitivity of the acoustics of short circular holes to inlet edge geometries

Dong Yang*, Juan Guzmán†, Holly G. Johnson‡ and Aimee S. Morgans§
Imperial College London, London SW7 2AZ, UK

Short circular holes with a low Mach number mean bias flow passing through them can absorb or generate acoustics. A recent semi-analytical model (Yang & Morgans, Journal of Sound and Vibration, 384 (2016) pp. 294-311 & 393 (2017) pp. 41-61) based on the Green's function method has been shown to be able to capture both the acoustic absorption and generation. The model indicates the importance of accurately capturing the path of the shed vorticity from the hole inlet edge. In the present work, the effect of this vorticity path on the hole acoustics is first studied systematically using the semi-analytical model. As the vorticity path is sensitive to the sharpness of the hole inlet edge, CFD tools are then used to obtain the vortex sheet shape after slightly changing the hole inlet edge shape. The acoustic responses of these modified holes are obtained using the semi-analytical model. A slightly chamfered edge case and a small ellipse edge case are considered to show that a very small change to the shape of the hole inlet edge can give a significant difference in the hole acoustic response.

I. Introduction

The sound absorption ("damping") or generation (or "whistling") of a short circular hole is relevant to many applications. Many practical situations involve a low Mach number mean flow passing through the holes, such as a cooling flow passing through perforated liners or Helmholtz resonators in aero-engine or land-based gas turbine combustors [1–6], fuel-air mixtures passing through injectors into combustors [7], and air from the lungs passing through the glottis [8].

At high Reynolds numbers, the viscous effect is small except in the vicinity of the hole edge. At low frequencies, significant acoustic damping occurs due to the conversion of acoustic energy into the sound induced unsteady shedding of vortices from the lip of the hole. Theoretical models dealing with this vortex-sound interaction usually assume that the shed vortices at the hole inlet edge are convected downstream by the mean flow to form a thin vortex sheet within the mean shear layer [9]. For an infinitely short circular hole with half spaces either side, Howe [10] assumed a downstream cylindrical vortex sheet with the same radius as the hole, neglected any shear layer instability, and then developed an analytical model which captures the acoustic dissipation well for very short holes [1].

When the hole length is of the same order as the hole radius but not long enough to allow the separated mean inlet flow to reattach within it (as shown in Fig. 1), the hole impedance was experimentally found to differ substantially from Howe's predictions [11]. Such holes were found to have the potential to generate as well as absorb acoustic energy, even in the low Strouhal number region. Recent semi-analytical models [12, 13] which account for the vortex-sound interactions both after and within the short hole revealed the importance of accurately capturing the path of the shed vorticity (or the vortex sheet shape). When the vortex path is captured accurately, the acoustic predictions agree well with previous experimental and CFD results, for example predicting both the absorption and generation of acoustics.

However, it is widely known that both the flow contraction coefficient – the minimum vortex sheet radius divided by the hole radius – and the precise vortex sheet shape near the hole inlet edge can be sensitive to the hole inlet edge sharpness [14]. This inspires us to modify (and eventually optimise) the hole acoustics by slightly modifying the hole inlet edges. In the present work, the semi-analytical model developed in [12, 13] is firstly used to systematically study the effect of the vortex sheet shape on the hole acoustics. Then, as the vortex sheet shapes are assumed unaffected by small acoustic perturbations [11], the vortex sheet shapes generated by different hole inlet edge geometries are obtained by incompressible RANS CFD solvers. Incorporating the vortex sheet shapes obtained from the numerical simulations

*Research Associate, Department of Mechanical Engineering
†Research Associate, Department of Mechanical Engineering
‡Research Associate, Department of Mechanical Engineering
§Professor, Department of Mechanical Engineering

into the semi-analytical model allows us to determine the effect of changing the hole inlet edge on the hole acoustic response.

II. Theoretical model

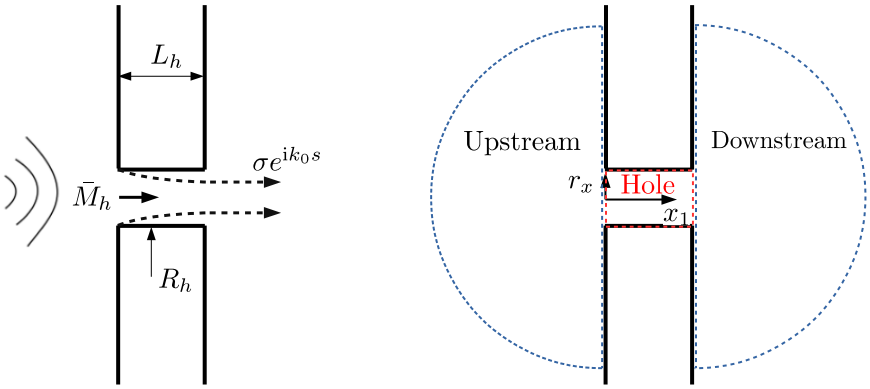


Fig. 1 (Left) A short circular hole opening to half spaces on either side with upstream incoming acoustic waves and the corresponding shed vortex sheet – $\sigma e^{ik_0 s}$ gives the strength and phase of the shed vorticity (σ) and its convection ($k_0 = \omega/|\boldsymbol{u_c}|$) along the vortex sheet path (s). (Right) Upstream, downstream and hole regions of the system.

A circular hole with a low Mach number mean flow, $\bar{M}_h$, passing through it from left to right is shown in Fig. 1 (left). The hole is assumed to open to half spaces either side. A detailed description of the theoretical method is given in [12, 13, 15]. To aid the reader, the main steps are outlined below. Neglecting viscosity, volume forces and entropy, the convected wave equation in stagnation enthalpy, B', for the acoustics of this system can be written as

$$\Big(\frac{1}{\bar{c}^2}\big(\frac{\partial}{\partial t} + \bar{u}\frac{\partial}{\partial x_1}\big)^2 - \nabla^2\Big)B' = \nabla\cdot(\boldsymbol{\omega}'\times\boldsymbol{u_c}), \tag{1}$$

where the mean velocity is assumed to be purely in the x_1 (axial) direction with value $\bar{u}$, and the vortex convection velocity is generally assumed to be equal to the mean velocity in the hole [1, 10, 16, 17] – we use $\boldsymbol{u_c}$ in the following to denote this mean vortex convection velocity. The flow is assumed to be homentropic with constant mean density and sound speed. The right hand side of Eq. (1) is the acoustic source term, with $\boldsymbol{\omega}'$ the oscillating vorticity [10, 18]. We introduce a Green's function which is defined in the frequency domain as $\widetilde{G}(\boldsymbol{x},\boldsymbol{y},\omega)$,

$$\Big(\frac{1}{\bar{c}^2}\big(-\mathrm{i}\omega + \bar{u}\frac{\partial}{\partial x_1}\big)^2 - \nabla^2\Big)\widetilde{G} = \delta(\boldsymbol{x}-\boldsymbol{y}), \tag{2}$$

where δ is the Dirac delta function. If we choose a space by using a Heaviside function H which equals 1 inside and 0 outside the space, combine Eqs.(1, 2), oscillations within the chosen space are then given by

$$\widetilde{B}(\boldsymbol{x},\omega)H = \int_S \Big(2\mathrm{i}k\bar{M}\widetilde{G}\widetilde{B}\,\boldsymbol{i} + \widetilde{G}\nabla\widetilde{B} - \widetilde{B}\nabla\widetilde{G}\Big)\cdot\mathrm{d}\boldsymbol{s} - \int_V (\widetilde{\boldsymbol{\omega}}\times\boldsymbol{u_c})\cdot\nabla\widetilde{G}\mathrm{d}v, \tag{3}$$

where V is the space volume and S denotes the surface bounding the volume.

Next, the whole system is split into three regions, as shown in Fig. 1 (right) – the region upstream of the hole, the region inside the hole and the region downstream of the hole. The Green's function which satisfies Eq. (2) can be obtained by incorporating boundary conditions for each region. For the large spaces both up- and downstream, a half space Green's function is used. Fourier Bessel expansions are used to obtain Green's functions inside the hole – this is explained in detail in [12].

By substituting the relevant Green's functions into Eq. (3), stagnation enthalpy oscillations in the three regions can be obtained. An incoming plane acoustic wave from far upstream is the only input acoustic wave to the system. Velocity oscillations at the hole inlet and outlet are unknown and are expanded as sums of a series of Bessel functions. The mean flow contraction gives a curved vortex sheet shape near the hole inlet edge which is discretized along its path into short

truncated cone rings. Once full expressions for the stagnation enthalpy oscillations near the hole inlet and outlet have been obtained, the oscillating hole inlet and outlet velocities follow by applying stagnation enthalpy continuity across the hole inlet and outlet interfaces. The vortex sheet strength and phase are obtained by imposing the Kutta condition at the hole inlet edge. Stagnation enthalpy oscillations in the up- and downstream regions can then be obtained as the linear function of only the incident plane wave far upstream. Considering only the plane wave oscillations ahead and downstream of the hole, the Rayleigh conductivity of the hole, which denotes the relation between the volume flux oscillation through the hole, $\widetilde{Q}$, and the acoustic pressure oscillation difference across it, $\Delta\widetilde{p}$, is finally obtained through

$$K_R = 2R_h(\Gamma_R - \mathrm{i}\Delta_R) = -\frac{\mathrm{i}\omega\bar{\rho}\widetilde{Q}}{\Delta\widetilde{p}}. \tag{4}$$

Note that R_h is the hole radius, Γ_R represents the inertia of the hole flow and is called the hole reactance and Δ_R, termed the resistance, is responsible for the absorption (Δ_R positive) or generation (Δ_R negative) of acoustic energy. This is because the acoustic energy absorbed by the hole, Π, can be calculated through $\Pi = \left\langle \mathrm{Real}(\Delta\widetilde{p}e^{-\mathrm{i}\omega t})\mathrm{Real}(\widetilde{Q}e^{-\mathrm{i}\omega t})\right\rangle$, where Real denotes real part and the angle brackets time average. It then follows that

$$\Pi = \frac{1}{4}(\Delta\widetilde{p}^*\widetilde{Q} + \widetilde{Q}^*\Delta\widetilde{p}) = \frac{R_h\Delta_R|\Delta\widetilde{p}|^2}{\omega\bar{\rho}}, \tag{5}$$

where $[\,]^*$ denotes the complex conjugate. Equation (5) shows that the acoustic energy absorption is determined by the imaginary part of the Rayleigh conductivity.

III. The effect of the vortex sheet shape

In [12, 13], the experimentally measured vortex sheet profile [19] for a hole opening towards semi-infinite spaces on both sides is used. However, it is widely known that the vortex sheet shape near the inlet edge is very sensitive to the hole inlet edge sharpness [11, 14]. In the following part of this section, we will study the effect of the vortex sheet shape on the Rayleigh conductivity of the hole. Firstly, we choose to parametrically model the vortex sheet shape using an exponential function of the form

$$y^* = 1 - a(1 - e^{-bx^*}), \tag{6}$$

where $y^* = R_V/R_h$ is the normalised radius, and $x^* = x_1/R_h$ the normalised axial location. Figure 2 shows that $a = 0.2$, $b = 6$ gives approximately the same shape as the experimental result in [19]. Slightly changing the values of a and b changes the vortex sheet shape slightly, as shown in Fig. 2.

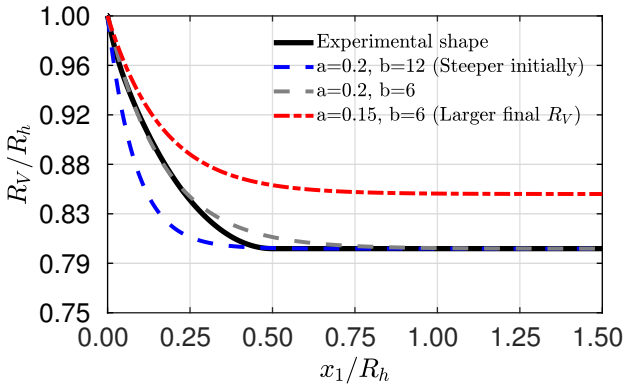


Fig. 2 Vortex sheet shapes. The experimental shape comes from [19], and the others come from Eq. (6) with different values for a and b.

Figure 3 compares the predicted real and imaginary parts of the Rayleigh conductivity with experimental data for a hole with $L_h/R_h = 1$. It can be clearly seen that at very low frequencies ($S_t < 0.4$), both the modified Howe's model and the present model with slightly different vortex sheet shapes capture the Rayleigh conductivity well. This is especially clear for Δ_R which is responsible for the acoustic absorption. For Γ_R, it should be noted that experimental errors become significant for very small Γ_R as the acoustic impedance is dominated by resistance (Δ_R) at very low

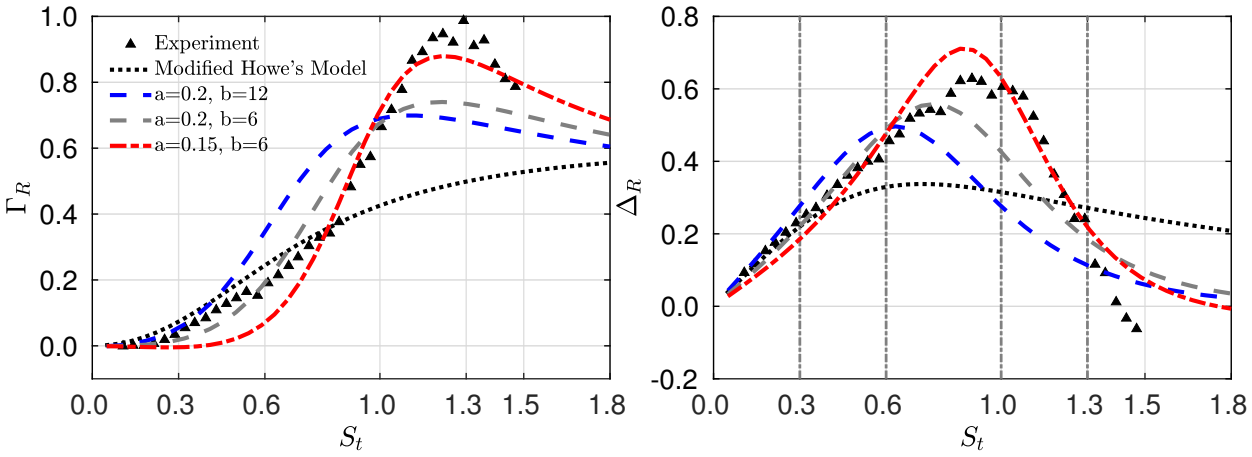


Fig. 3 Γ_R **and** Δ_R **of the Rayleigh conductivity, with** $L_h/R_h = 1$**. Dimensionless frequency is** $S_t = \omega R_h/|\boldsymbol{u_c}|$**. Results with different** a **and** b **come from the present model using vortex sheet shapes in Fig. 2. Experimental results are from Su et al. [11], and the modified Howe's model [10] applies a compact hole mass inertial correction [20]. Gray dash-dot lines show the frequencies at which a systematic study into the effect of changing** a **and** b **is performed in Fig. 4**

frequencies. For $S_t > 0.4$, the experimental Γ_R and Δ_R start to exhibit very different trends to those predicted by the modified Howe's model. Both exhibit much larger growths between $0.4 < S_t < 1$. As the frequency further increases, the experimental Γ_R decreases slightly beyond $S_t > 1.2$ while Δ_R decreases dramatically beyond $S_t > 1.1$ – even to negative values when $S_t > 1.4$ which means the hole is generating rather than absorbing acoustics. None of these important trends are captured by the modified Howe's model, but are both captured by the present model – the negative Δ_R can be captured if a proper vortex sheet shape or a longer hole is used, as discussed in [12, 13]. Note that the actual vortex sheet shape for the experiment in [11] is unknown, but the results in Fig. 3 suggest that the parametric representation of Eq. (6) with $a = 0.15$, $b = 6$ is a better estimate, rather than the measured shape from [19].

Figure 3 also shows that both Γ_R and Δ_R are sensitive to the shape of the vortex sheet – Γ_R is sensitive over the whole considered S_t range, while Δ_R shows most sensitivity in the frequency range $0.6 < S_t < 1.5$. The effect of changing a and b (and thus the vortex sheet shape) on Δ_R at four different frequencies (S_t) is shown for a large range of a and b in Figs. 4 and 5. Generally, a larger variation of Δ_R is observed at higher S_t, meaning that the acoustic response is more sensitive to the vortex sheet shape variations at higher frequencies. It is clear that for a given frequency, certain combinations of a and b lead to a peak in absorption, with these combinations dependent on frequency. This indicates that the optimum vortex sheet shape varies strongly on the frequency of interest.

It is also worth mentioning that negative Δ_R is seen at $S_t = 1.3$ for the longer hole considered in Fig. 4 but not for the shorter hole considered in Fig. 5. This is because a longer hole is more likely, than a shorter hole, to generate acoustics, this being consistent with results from [12, 13, 17, 21, 22].

IV. Modifying vortex sheet shapes by slightly changing hole inlet edges

It is clear that different vortex sheet shapes can give very different hole acoustic responses. In this section, we will show how such different vortex sheets can be obtained by only very slight modifications to the hole inlet edge. To this end, incompressible RANS simulations will be used. This approach is consistent with the assumption that acoustic perturbations have negligible effect on the vortex sheet shape near the hole [11].

The computational domain is composed of three sequential concentric cylinders. The first is placed in the left part of the domain with the flow inlet corresponding to its left base and its length 885 mm. To its right is a shorter cylinder corresponding to the hole of interest and whose radius measures 5 mm. Downstream (to the right) of the hole, there is a large cylindrical plenum of length 687 mm and radius 120 mm. Both the length of the hole and the radius of the inlet duct are varied to obtain different L_h/R_h and hole opening expansion ratios, respectively. Due to the axisymmetric nature of the problem and boundary conditions, the flow is solved in a wedge domain with periodic boundary conditions in the azimuthal direction.

To calculate the mean flow, the incompressible RANS equations are converged to a steady state using the finite

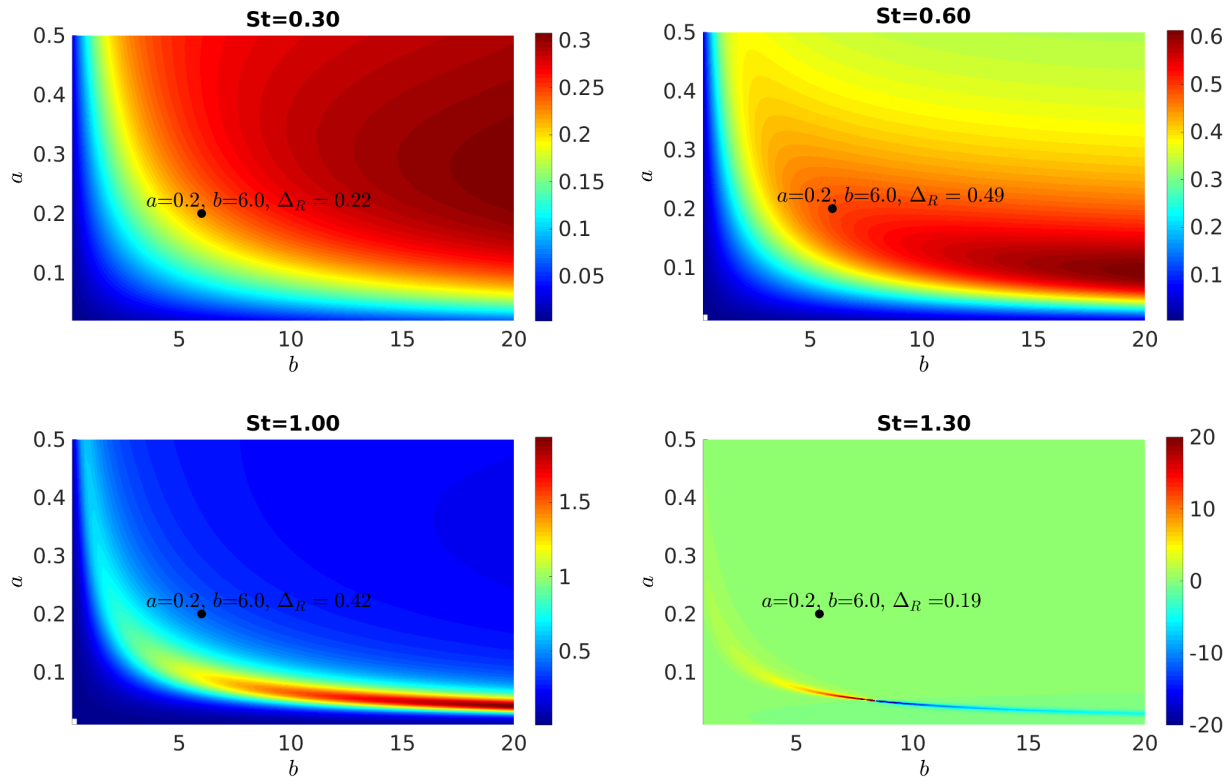


Fig. 4 Contour plot of Δ_R, with $L_h/R_h = 1$ – the imaginary part of the Rayleigh conductivity, at several frequencies. a and b are coefficients in Eq. (6).

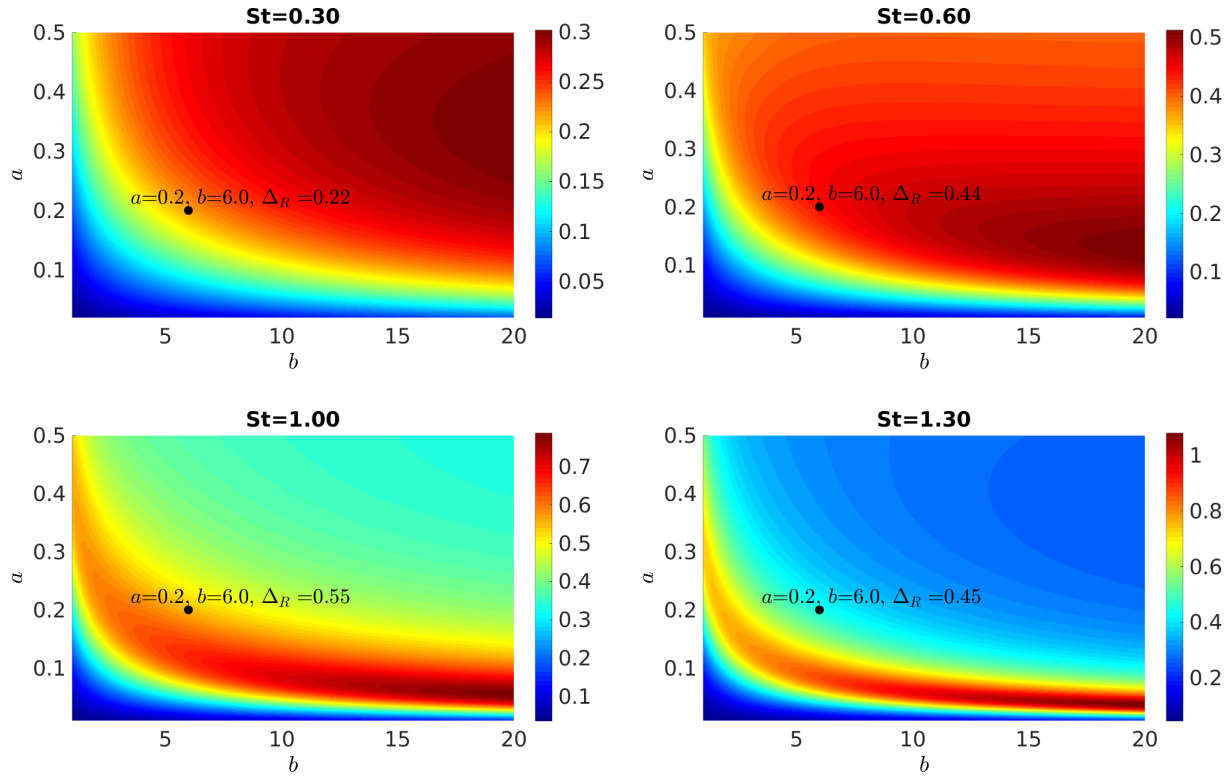


Fig. 5 Contour plot of Δ_R, with $L_h/R_h = 0.5$ – the imaginary part of the Rayleigh conductivity, at several frequencies. a and b are coefficients in Eq. (6).

volume solver OpenFoam. The mean pressure drop was set to 500 Pa . The transport properties are those standard for air at room temperature; i.e. $\rho = 1.22\ kg/m^3$ and $\nu = 1.5 \times 10^{-5} m^2/s$. The inlet normal velocity is varied to obtain three Reynolds numbers: $Re = 2\rho\bar{U}R_h/\mu = 10^4, 2 \times 10^4$ and 4×10^4. The adopted turbulence model is the Menter k–ω shear-stress-transport (SST) model due to its performance for free-shear and wall-bounded flows. A SIMPLE algorithm is used to solve the momentum and pressure correction equations. A non-slip boundary condition is imposed at the hole walls and a symmetry condition is imposed on the external walls of both the inlet duct and plenum.

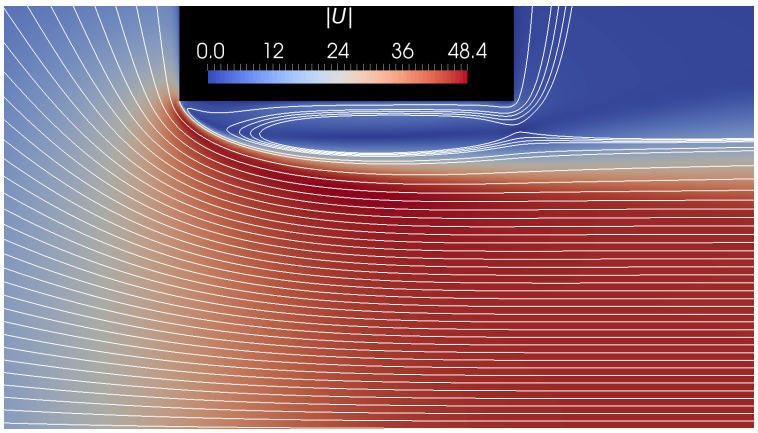


Fig. 6 Contour plot for the absolute value of the axial velocity, $|U|$ for the straight hole inlet edge case. The flow separates at the hole inlet edge, with white lines denoting the stream lines.

We first study the effect of the hole opening expansion ratio, the mean flow Reynolds number, and the hole length for the non-modified/straight-edge geometry. Figure 6 shows the mean flow profile of an unmodified straight (inlet edge) hole. The vortex sheet shape can be approximately denoted by the largest azimuthal vorticity [23], the center radius of the shear layer, or the streamline from the flow separation point (which is the edge for the present case) – the last is used in the present paper. The hole is assumed to open to a large space downstream (with a radius expansion ratio of 12), with the opening confinement upstream varying across radius expansion ratio from $\lambda = 5$ to 20 ($L_h/R_h = 1$ and $Re = 2 \times 10^4$). Results in Fig. 7 (Top left) show that the upstream expansion ratio does not noticeably affect the vortex sheet shape when it is larger than ~ 5, agreeing with experimental results [19]. In Fig. 7 (Top right), λ is fixed to 5 and $L_h/R_h = 1$. At these high Reynolds numbers (common in acoustic dampers for aero-engine and land-based gas turbines), the vortex sheet shape is not sensitive to the variation of Reynolds number. However, Fig. 7 (bottom), with $\lambda = 5$ and $R_e = 1 \times 10^4$, clearly shows that varying the hole length between $0.5 \leq L_h/R_h \leq 2$ can significantly change the vortex sheet shape. In the following parts of the present paper, we consider only the $L_h/R_h = 0.5$ case – this gives a nearly straight vortex sheet tail for $x_1/R_h \geq 0.5$ and thus allows us to use the two parameter expression in Eq. (6) for modelling. Note that more complex vortex sheet shapes could be considered by the present semi-analytical model – the only requirement is that the hole is not long enough to allow mean flow reattachment [12, 13].

The $\lambda = 5$, $R_e = 2 \times 10^4$ and $L_h/R_h = 0.5$ case is now used to study hole inlet edge modifications. A chamfered and an ellipse edge are considered, as shown in Fig. 8, with the modification $\delta_l/R_h \approx 2\%$ being very small. The mesh near the edge is carefully refined to make sure that the flow separation is accurately captured. To this end a sensitivity analysis of the mesh in that region has been systematically performed.

Even though the edge modifications are very small, the extracted vortex sheet shapes in Fig. 9 exhibit noticeable difference compared to the straight case – confirming high sensitivity to the hole inlet edge shape. The vortex sheet shape from the straight edge case agrees approximately with the experimental result from [19], while the chamfered and ellipse cases both give a less contracted shape. Note that the difference between the chamfered and ellipse case is small but noticeable, and changing the ratio between the two axes of the ellipse or the two laterals of the chamfered edge leads to further variations.

Equation (6) is then used to fit these vortex sheet shapes with the fitted results plotted in Fig. 9 with $a = 0.186$, $b = 6.82$ for the straight case, $a = 0.159$, $b = 4.92$ for the chamfered case, $a = 0.166$, $b = 5.2$ for the ellipse case, and $a = 0.199, b = 6.15$ for the experimental result. It can be seen that the shapes for the chamfered and ellipse cases are well captured by the corresponding fitted curves, although with slight differences near the edge.

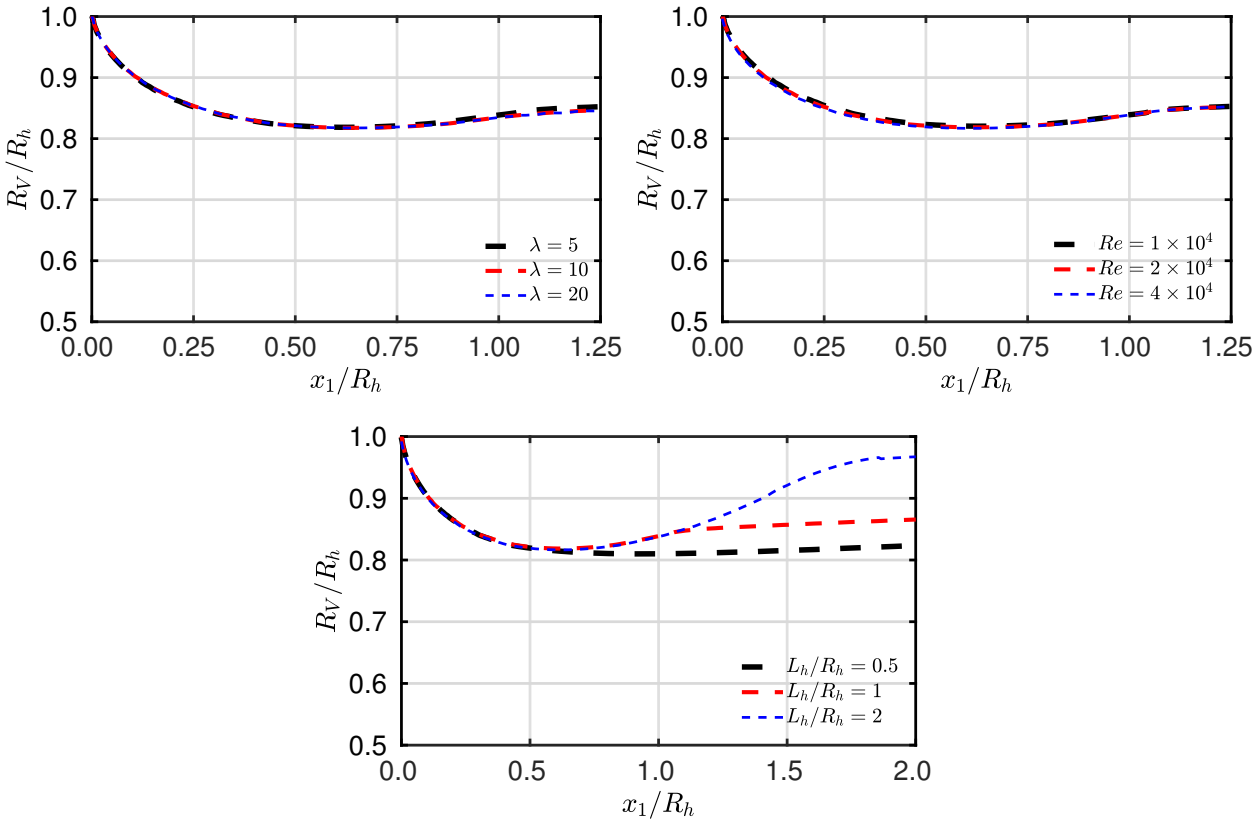


Fig. 7 Vortex sheet shapes for (Top left) different expansion ratios at the upstream side, (Top right) different mean flow Reynolds numbers $Re = 2\rho\bar{U}R_h/\mu$, and (Bottom) different hole lengths.

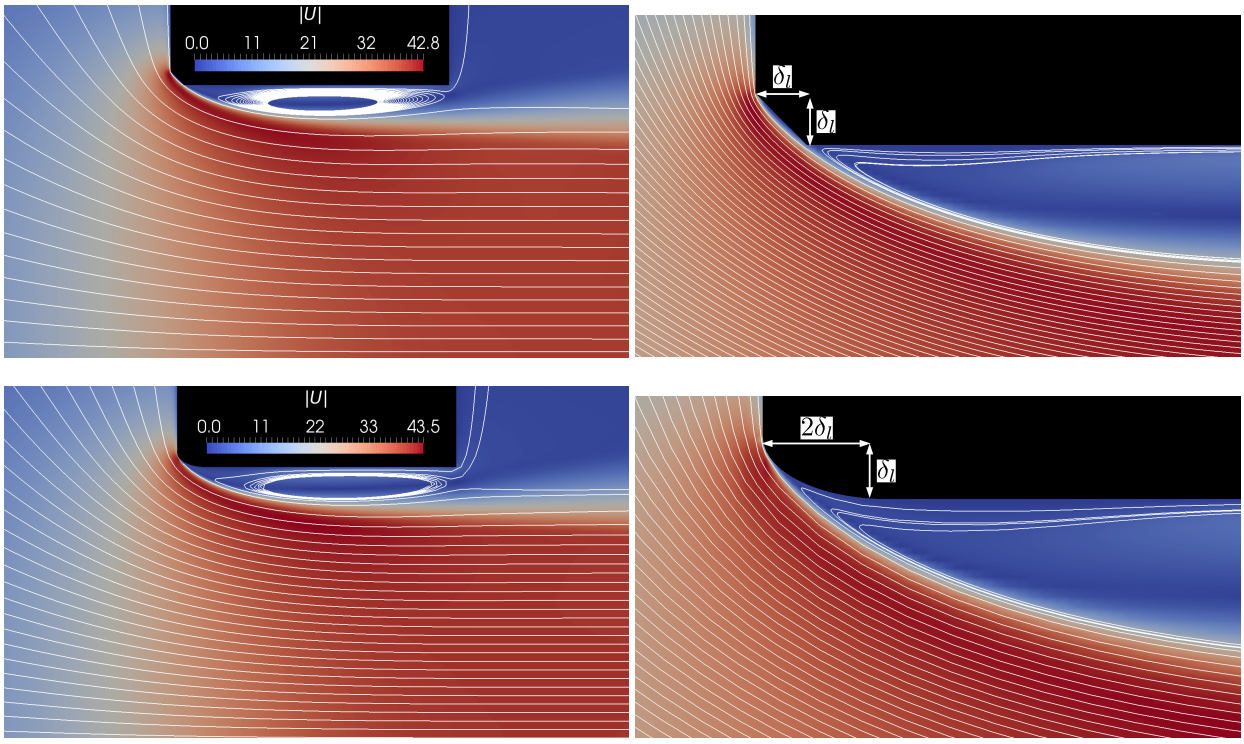


Fig. 8 Contour plot for the absolute value of the axial velocity, $|U|$, with white lines denoting the stream lines. (Top left) A chamfered hole case, with (Top right) a zoomed-in view near the inlet edge. (Bottom left) An ellipse hole case, with (Bottom right) a zoomed-in view near the inlet edge.

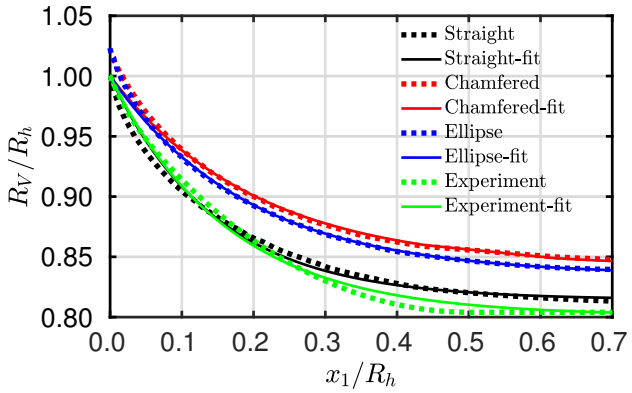


Fig. 9 Vortex sheet shapes of different hole inlet edge shapes. $L_h/R_h = 0.5$. The dotted lines are results from CFD simulations and the fitted results assume the vortex sheet shape form in Eq. (6) with different values of a and b calculated by using a least squares method. The experiment shape comes from [19].

V. Acoustics of the modified holes

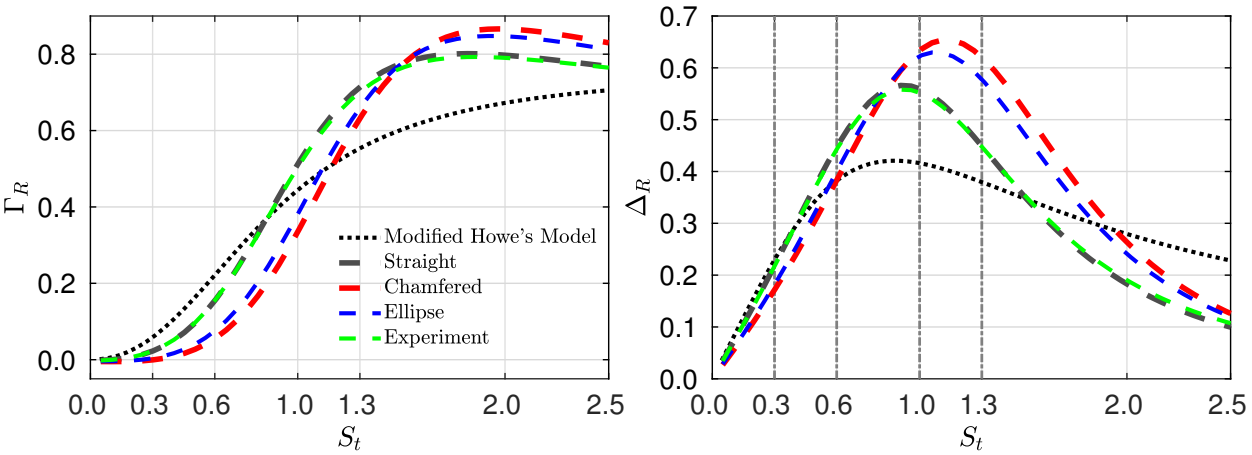


Fig. 10 Γ_R and Δ_R of the Rayleigh conductivity for holes with different inlet edge shapes. $L_h/R_h = 0.5$. Dimensionless frequency is $S_t = \omega R_h/|\boldsymbol{u_c}|$. Experimental results consider the experimental vortex sheet shape from [19], and the modified Howe's model [10] applies a compact hole mass inertial correction [20]. Gray dash-dot lines show the frequencies at which a systematic study into the effect of changing a and b was performed in Fig. 5.

The acoustic responses for the three hole inlet edges are now studied by incorporating their fitted vortex sheet shapes into the present semi-analytical model. The Rayleigh conductivities across a wide range of frequencies are shown in Fig. 10. As expected, the straight hole gives very similar Rayleigh conductivities (both Γ_R and Δ_R) to the experimental vortex sheet shape case. Both the chamfered and ellipse holes give significantly different results compared to the straight hole even though their edge modification is small. This is especially true for Δ_R in the frequency range $1 \leq S_t \leq 2 - \Delta_R$ for the modified holes can be 30% $\sim$ 50% larger than the straight hole case, meaning that the sound absorption can be 30% $\sim$ 50% higher. The hole reactance part, Γ_R, can be much lower than that of the straight hole at $S_t \leq 1.3$ (10% $\sim$ 80% depending on its absolute value at different S_ts) – note that when the hole Rayleigh conductivity is included into a Helmholtz resonator model, accurate knowledge of this reactance is important for accurately predicting the resonator's resonant frequency [2, 6, 13, 24]. It is also worth mentioning that the modified Howe's model, which cannot consider detailed vortex sheet shapes, gives very different real and imaginary parts of the Rayleigh conductivity compared to the present model.

VI. Conclusions

The present paper provides a theoretical and numerical study into the sensitivity of the acoustics of short circular holes to inlet edge geometries. This is done by modifying the acoustics of short circular holes through slightly changing their inlet edges. The theoretical part relies on a recently developed semi-analytical model which resolves the detailed vortex-sound coupling for short circular holes with a mean bias flow. This makes the study of the acoustic response of holes with different vortex sheet shapes very efficient. As the vortex sheet shape is very sensitive to the shape of the hole inlet edge, but assumed insensitive to acoustic perturbations, an efficient incompressible RANS simulation is used to extract the vortex sheet shapes with small hole inlet edge modifications. By combining these two parts, the present study shows that very small changes of the hole inlet edge can bring about significant variations in the vortex sheet shape, and corresponding significant modifications to the hole acoustic response. The present paper provides a very efficient tool to study this problem and paves the way to systematically optimise the acoustics of short circular holes by modifying their inlet edge shapes.

References

[1] Eldredge, J. D., and Dowling, A. P., "The absorption of axial acoustic waves by a perforated liner with bias flow," *Journal of Fluid Mechanics*, Vol. 485, 2003, pp. 307–335.

[2] Dupère, I. D. J., and Dowling, A. P., "The use of Helmholtz resonators in a practical combustor," *Journal of Engineering for Gas Turbines and Power*, Vol. 127, No. 2, 2005, pp. 268–275.

[3] Zhao, D., and Li, X. Y., "A review of acoustic dampers applied to combustion chambers in aerospace industry," *Progress in Aerospace Sciences*, Vol. 74, 2015, pp. 114–130.

[4] Ni, F., Miguel-Brebion, M., Nicoud, F., and Poinsot, T., "Accounting for acoustic damping in a helmholtz solver," *AIAA Journal*, 2016, pp. 1–16.

[5] Yang, D., Wang, X., and Zhu, M., "The impact of the neck material on the sound absorption performance of Helmholtz resonators," *Journal of Sound and Vibration*, Vol. 333, No. 25, 2014, pp. 6843–6857.

[6] Yang, D., and Morgans, A. S., "Acoustic Models for Cooled Helmholtz Resonators," *AIAA Journal*, Vol. 55, No. 9, 2017, pp. 3120–3127.

[7] Candel, S., Durox, D., Schuller, T., Bourgouin, J.-F., and Moeck, J. P., "Dynamics of swirling flames," *Annual Review of Fluid Mechanics*, Vol. 46, 2014, pp. 147–173.

[8] Howe, M. S., and McGowan, R. S., "Production of sound by unsteady throttling of flow into a resonant cavity, with application to voiced speech," *Journal of Fluid Mechanics*, Vol. 672, 2011, pp. 428–450.

[9] Howe, M. S., "Attenuation of sound in a low Mach number nozzle flow," *Journal of Fluid Mechanics*, Vol. 91, No. 02, 1979, pp. 209–229.

[10] Howe, M. S., "On the theory of unsteady high Reynolds number flow through a circular aperture," *Proceedings of the Royal Society of London. A. Mathematical and Physical Sciences*, Vol. 366, No. 1725, 1979, pp. 205–223.

[11] Su, J., Rupp, J., Garmory, A., and Carrotte, J. F., "Measurements and computational fluid dynamics predictions of the acoustic impedance of orifices," *Journal of Sound and Vibration*, Vol. 352, 2015, pp. 174–191.

[12] Yang, D., and Morgans, A. S., "A semi-analytical model for the acoustic impedance of finite length circular holes with mean flow," *Journal of Sound and Vibration*, Vol. 384, 2016, pp. 294–311. doi:10.1016/j.jsv.2016.08.006.

[13] Yang, D., and Morgans, A. S., "The acoustics of short circular holes opening to confined and unconfined spaces," *Journal of Sound and Vibration*, Vol. 393, 2017, pp. 41–61. doi:10.1016/j.jsv.2016.12.027.

[14] Bullen, P. R., Cheeseman, D. J., and Hussain, L. A., "The effects of inlet sharpness on the pipe contraction pressure loss coefficient," *International Journal of Heat and Fluid Flow*, Vol. 9, No. 4, 1988, pp. 431–433.

[15] Yang, D., "The acoustics of short circular holes and their damping of thermoacoustic oscillations," Ph.D. thesis, 2017.

[16] Hughes, I. J., and Dowling, A. P., "The absorption of sound by perforated linings," *Journal of Fluid Mechanics*, Vol. 218, 1990, pp. 299–335.

[17] Jing, X., and Sun, X., "Effect of plate thickness on impedance of perforated plates with bias flow," *AIAA Journal*, Vol. 38, No. 9, 2000, pp. 1573–1578.

[18] Dupère, I. D. J., and Dowling, A. P., "The absorption of sound near abrupt axisymmetric area expansions," *Journal of Sound and Vibration*, Vol. 239, No. 4, 2001, pp. 709–730.

[19] Rouse, H., and Abul-Fetouh, A., "Characteristics of irrotational flow through axially symmetric orifices," *Journal of Applied Mechanics-Transactions of the ASME*, Vol. 17, No. 4, 1950, pp. 421–426.

[20] Jing, X., and Sun, X., "Experimental investigations of perforated liners with bias flow," *The Journal of the Acoustical Society of America*, Vol. 106, No. 5, 1999, pp. 2436–2441.

[21] Lacombe, R., Moussou, P., and Aurégan, Y., "Whistling of an orifice in a reverberating duct at low Mach number," *The Journal of the Acoustical Society of America*, Vol. 130, No. 5, 2011, pp. 2662–2672.

[22] Kierkegaard, A., Allam, S., Efraimsson, G., and Åbom, M., "Simulations of whistling and the whistling potentiality of an in-duct orifice with linear aeroacoustics," *Journal of Sound and Vibration*, Vol. 331, No. 5, 2012, pp. 1084–1096.

[23] Mendez, S., and Eldredge, J. D., "Acoustic modeling of perforated plates with bias flow for large-eddy simulations," *Journal of Computational Physics*, Vol. 228, No. 13, 2009, pp. 4757–4772.

[24] Bellucci, V., Flohr, P., Paschereit, C. O., and Magni, F., "On the use of Helmholtz resonators for damping acoustic pulsations in industrial gas turbines," *Journal of Engineering for Gas Turbines and Power*, Vol. 126, No. 2, 2004, pp. 271–275.